BIOPHYSICS

Molecular mechanism of extreme mechanostability in a pathogen adhesin

Lukas F. Milles,[1] Klaus Schulten,[2]* Hermann E. Gaub,[1]† Rafael C. Bernardi[2]†

High resilience to mechanical stress is key when pathogens adhere to their target and initiate infection. Using atomic force microscopy–based single-molecule force spectroscopy, we explored the mechanical stability of the prototypical staphylococcal adhesin SdrG, which targets a short peptide from human fibrinogen β. Steered molecular dynamics simulations revealed, and single-molecule force spectroscopy experiments confirmed, the mechanism by which this complex withstands forces of over 2 nanonewtons, a regime previously associated with the strength of a covalent bond. The target peptide, confined in a screwlike manner in the binding pocket of SdrG, distributes forces mainly toward the peptide backbone through an intricate hydrogen bond network. Thus, these adhesins can attach to their target with exceptionally resilient mechanostability, virtually independent of peptide side chains.

Gram-positive pathogenic bacteria have developed an arsenal of virulence factors specifically targeting and adhering to their host's proteins. Termed microbial surface components recognizing adhesive matrix molecules (MSCRAMMs), they promote "adhesion, invasion, and immune evasion" (*1*) (Fig. 1A). The prototypical adhesin is SD-repeat protein G (SdrG) from *Staphylococcus epidermidis*, the leading cause of medical device– and implant-related nosocomial infections (*2*). SdrG uses a key motif found in pathogenic staphylococci—the "dock, lock, and latch" (DLL) mechanism—in which the host target, usually a peptide on the order of 15 residues, is first bound (dock), then buried (lock) between two immunoglobulin-like (Ig) fold domains N2 and N3 (*3*). Finally, the target is snugly locked in place with a strand connecting N3 to N2 by β-strand complementation (latch) (Fig. 1B) (*4*). The DLL mechanism has appeared in many homologous domains—for example, in *Staphylococcus aureus* with targets such as keratin (*5*), complement system proteins (*6*), other chains of fibrinogen (*7*) and collagen (*8*). SdrG uses the DLL to target the N terminus of the β chain of human fibrinogen (Fg). The Fg sequence bound by SdrG is also the substrate of thrombin (Fgβ, NEEGFFSA**RG**HRPLD, thrombin cleavage between R and G). However, once bound by SdrG, it can no longer be cut by thrombin, a step necessary for blood clotting and fibrin formation (*9*). Thrombin cleavage also releases fibrinopeptide B, which in turn recruits neutrophils. Additionally, the adhesin coats and thus camouflages the bacterium in host proteins. Combined, these MSCRAMM mechanisms allow staphylococci to evade immune response, making them attractive targets for drug development, such as designing MSCRAMM inhibitors for antiadhesion therapy (*10*, *11*).

Here, we use the interplay between atomic force microscopy (AFM)–based single-molecule force spectroscopy (SMFS) (*12*–*14*) and all-atom steered molecular dynamics (SMD) simulations to elucidate the mechanics of the SdrG:Fgβ interaction with atomic resolution. Previous in vivo measurements using single-cell force spectroscopy of the SdrG fibrinogen interaction found adhesion forces on the order of 2 nN (*15*, *16*); in addition, comparable in vivo forces appeared in closely related adhesins (*17*, *18*). In agreement with these results, we measured rupture forces of more than 2 nN for a single SdrG:Fgβ complex at force loading rates around 10^5 pN s^{-1}. This extreme stability is the highest among all noncovalent interactions by a large margin. SdrG:Fgβ outperforms the current champion—the cohesin-dockerin type III interaction—by a factor of four (*19*) and Biotin-Streptavidin by more than an order of magnitude (*20*). It even rivals the strength of a covalent bond (*21*). Interestingly, the affinity between the peptide and SdrG is moderate, with a dissociation constant (K_d) ~400 nM (*4*). Accordingly, this system is adapted for strong mechanical attachment to its target, rather than high affinity. It was thus to be expected that these extreme SdrG:Fgβ mechanics were governed by a special, currently unknown mechanism.

The Fgβ wild-type (WT) peptide is located at the N terminus of the mature Fgβ chain. Thus, it can only be mechanically loaded from the C terminus (Fig. 1B). The SdrG N2 and N3 domains, responsible for binding the peptide (SdrG), are covalently anchored to the *S. epidermidis* cell wall by a C-terminal sortase motif. Hence, in the native, physiological configuration of the SdrG:Fgβ complex, force is applied from the C termini of both SdrG and Fgβ. To mechanically probe this interaction, all surface anchoring onto AFM cantilever and surface was site-specific and covalent (Fig. 1C). To ensure unambiguous identification of single-molecule events in force-extension traces, a refolding molecular "fingerprint" (*22*) was cloned adjacent to the peptide. Under physiologically relevant direction of force application from the C terminus, the complex withstood extremely high forces of up to 2500 pN in vitro (Fig. 1, D and E) and even higher forces in corresponding SMD simulations (Fig. 1, F and G), due to higher force loading rates in silico (*23*, *24*) (see also figs. S1 to S3).

The force regime around 2 nN is typically associated with the stability of covalent bonds, raising the concern that our surface chemistry—not the complex—was breaking, most likely a Si-C bond in the aminosilane anchors used (*21*). Because the cantilevers' apexes have radii of ~10 nm, they can only present a few molecules. If the covalent attachment of SdrG to the tip was being mechanically cleaved, the SdrG coating on the apex of the tip would be left attached to the surface, resulting in a rapidly decreasing frequency of interactions over time. In contrast, a single cantilever remained active over thousands of interactions, indicating that covalent bonds in the surface functionalization largely sustained the high forces.

We were convinced that an alteration that lowered the unbinding force would be the key to deconstructing the mechanism of this exceptional mechanostability. The presence of the "bulky" hydrophobic amino acid side chains of two phenylalanines (F) in Fgβ had been previously described as a "bulgy plug" (*4*). Buried behind the locking β strand, it seemed conceptually and intuitively plausible that wiggling them through the narrow constriction created by the locking strand caused the high forces (Fig. 2, A and B, and fig. S4).

The force dependence on the number of Fs was tested by addition of an F or by alanine replacement. Four constructs were investigated: a Fgβ with three phenylalanines (FgβF3), the WT Fgβ having 2 Fs, and mutants with one (FgβF1), or both (FgβF0), Fs replaced by alanines. The F3 mutant had been shown to have higher affinity (K_d ~50 nM) for SdrG (*4*), whereas the affinity of the F1 mutant was lower compared to WT Fgβ, because the F's hydrophobicity is important for initiating the DLL (*25*). All three mutants produced high forces around 2 nN (fig. S5, A and B). A negative correlation of the most-probable rupture force on the number of Fs was measurable but only marginal (Fig. 2C). With reference to the Fgβ WT force, the most-probable rupture force of the F0 mutant was only about 10% weaker than the WT. Multiple all-atom SMD simulations of all four systems reproduced the miniscule correlation between the presence of bulky F side chains and the high forces (Fig. 2B). The F0 mutant was ~20% weaker than WT Fgβ. Thus, the bulky residues only contributed marginally to the high forces, whereas they had been established as crucial for initial binding (*4*).

As the bulky phenylalanines in Fgβ were largely irrelevant for reaching high forces, we investigated minimizing the peptide. We employed QwikMD (*26*) to sequentially remove amino acids from the N terminus of Fgβ and tested their stability in SMD simulations. As expected, shortened peptides had lower unbinding forces. However,

[1]Lehrstuhl für Angewandte Physik and Center for Nanoscience, Ludwig-Maximilians-University, Amalienstrasse 54, 80799 Munich, Germany. [2]NIH Center for Macromolecular Modeling and Bioinformatics, Beckman Institute for Advanced Science and Technology, University of Illinois at Urbana-Champaign, Urbana, IL 61801, USA.
*Deceased.
†Corresponding author. Email: rcbernardi@ks.uiuc.edu (R.C.B.); gaub@lmu.de (H.E.G.)

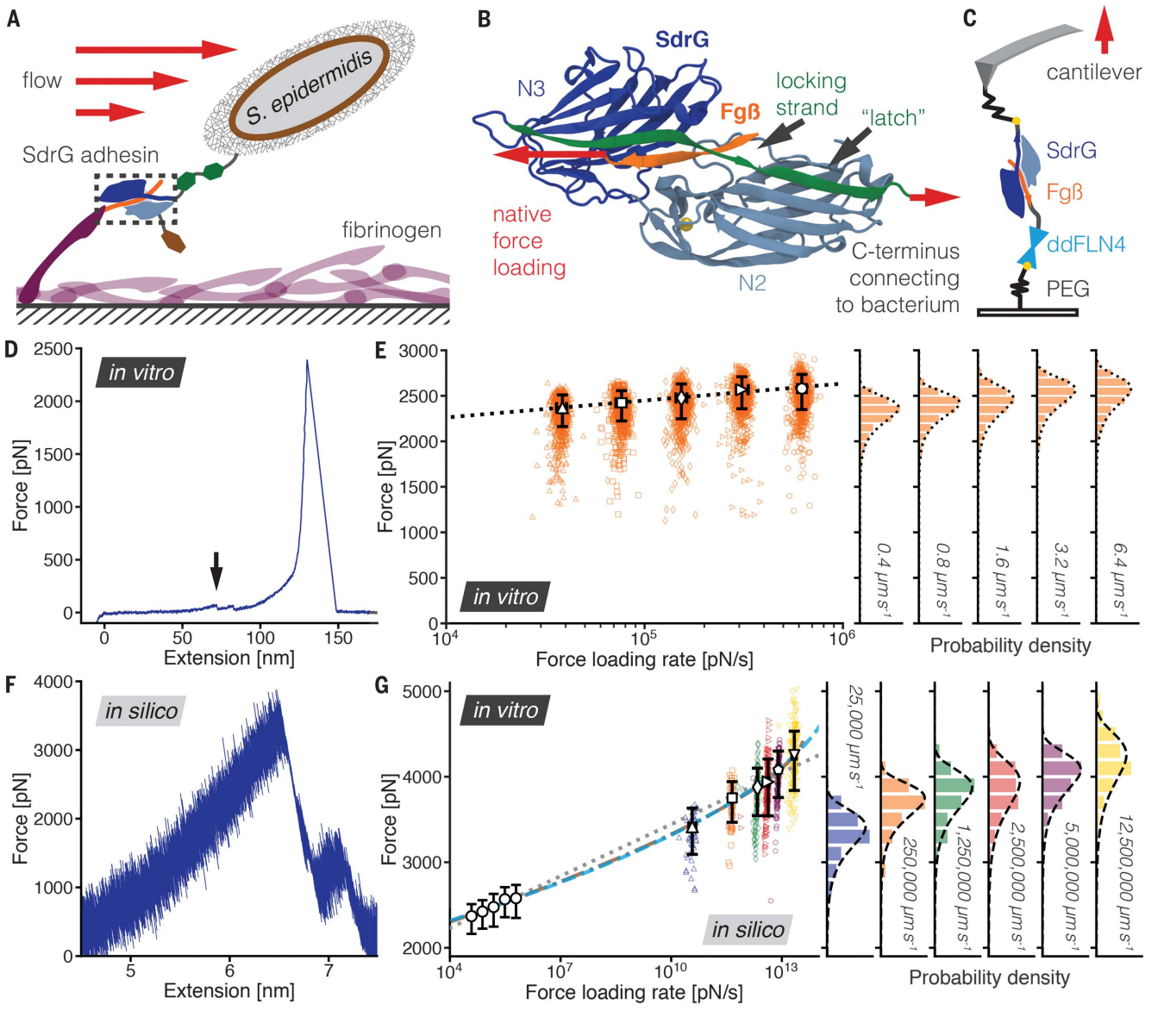

Fig. 1. The SdrG:Fgβ complex withstands enormous forces in vitro and in silico. (**A**) SdrG function, attached to the N-terminal peptide of the fibrinogen (purple) β chain (orange) adsorbed on a surface. This interaction prevents detachment of the bacterium by hydrodynamic forces. (**B**) Structure of the SdrG (blue):Fgβ (orange) complex. The locking strand (green) encloses the peptide in the binding pocket between the Ig-fold N2 (light blue) and N3 (dark blue) domain and a calcium (yellow) binding loop. The red arrows indicate the force applied to the molecular complex. (**C**) Experimental AFM setup, including the ddFLN4 fingerprint domain (cyan). All constructs are covalently bound to the surface via polyethyleneglycol (PEG) linkers and the ybbR-tag (yellow dots). In the native configuration, Fgβ and SdrG are force-loaded from their respective C termini. The AFM cantilever is retracted at constant velocity until the complex breaks. (**D**) Resulting force-extension trace in the native force propagation (blue), as it would occur at sites of staphylococcal adhesion. The distinctive fingerprint unfolding around 90 pN ddFLN4 (black arrow) featuring a substep was used to find specific interactions. It is followed by SdrG:Fgβ complex rupture, here at almost 2500 pN. (**E**) Dynamic force spectrum of the SdrG:Fgβ native geometry at cantilever retraction velocities 0.4 μm s^{-1} (triangles, N = 749), 0.8 μm s^{-1} (squares, N = 696), 1.6 μm s^{-1} (diamonds, N = 758), 3.2 μm s^{-1} (forward triangles, N = 749), 6.4 μm s^{-1} (circles, N = 851), with corresponding complex rupture-force histograms for each velocity projected onto individual axes on the right. A Bell-Evans (BE) model fit (dotted line, Δx = 0.051 nm, k_{off}^0 = 9.2 × 10^{-11} s^{-1}) through the most-probable rupture force and force loading rate of each velocity (large open markers, with errors given as full-width at half maximum for each distribution) shows the expected force loading-rate dependency of the rupture force. (**F**) SMD force-extension trace (blue) in the native force propagation of SdrG:Fgβ, including experimental peptide linkers. The complex ruptured at almost 4000 pN; the extension is shorter than in the experimental trace because there are no PEG spacers. The peak following the highest force peak corresponds to another metastable geometry after slipping of the Fgβ peptide that is below the resolution limit of our AFM. (**G**) The experimentally determined dynamic force spectrum from velocities of 0.4 to 6.4 μm s^{-1} for the native propagation from (E) is shown condensed as open circles. The dynamic force spectrum of SMD simulations for velocities of 25,000 μm s^{-1} to 12,500,000 μm s^{-1}, triangle N = 49, square N = 50, diamond N = 100, forward triangle N = 200, pentagon N = 147, inverted triangle N = 200, respectively. Fits through SMD and experimental data, for BE model (gray, dotted line, Δx = 0.047 nm, k_{off}^0 = 1.0 × 10^{-9} s^{-1}) and fit of a model by Dudko *et al*. (DHS model, cusp potential Δx = 0.12 nm, k_{off}^0 = 6.1 × 10^{-22} s^{-1}, ΔG^{++} = 78 k_BT, cyan dashed line and linear-cubic potential Δx = 0.093 nm, k_{off}^0 = 7.7 × 10^{-18} s^{-1}, ΔG^{++} = 66 k_BT, brown dash-dotted line, both at T = 300 K). In vitro and in silico data agree exceptionally well, although they are separated by six orders of magnitude in force loading rate and can be fit with a single model.

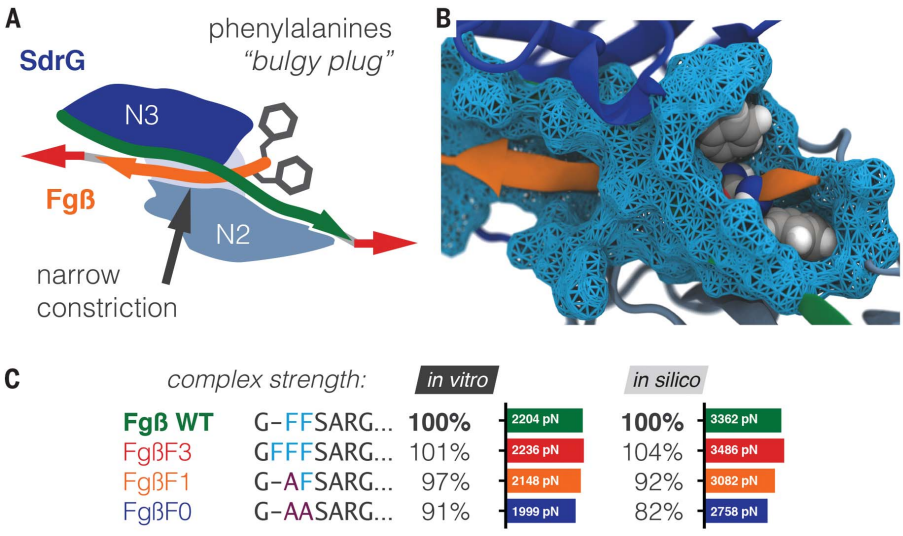

Fig. 2. Phenylalanine side chains only marginally influence SdrG:Fgβ mechanostability. (**A**) Sketch of the "bulgy plug" hypothesis. The bulky phenylalanine side chains (gray) of Fgβ (orange) are blocked by the locking strand (green). (**B**) Crystal structure showing the bulky phenylalanine side chains in van der Waals representation (gray spheres) of Fgβ (orange). They have to wiggle through a narrow constriction (cyan surface). (**C**) Dependence of complex rupture force on the presence of phenylalanines, if replaced by alanines. Most-probable rupture forces (absolute values in bar graphs) are compared relative to WT Fgβ. Either recorded experimentally with a single cantilever retracted at 1.6 μm s^{-1} or corresponding results for SMD simulations at 250,000 μm s^{-1}. Adding one F (FgβF3 mutant) slightly increases forces. Yet, both results show a trend of weak dependence of rupture force on the presence of phenylalanines. Even when removing all bulky side chains (FgβF0 mutant), experimental rupture forces drop no more than 10% compared with WT Fgβ; in silico, no more than 20%. The "bulgy plug" only marginally contributes, hinting that another mechanism must be responsible for the high forces. Single-letter abbreviations for the amino acid residues are as follows: A, Ala; C, Cys; D, Asp; E, Glu; F, Phe; G, Gly; H, His; I, Ile; K, Lys; L, Leu; M, Met; N, Asn; P, Pro; Q, Gln; R, Arg; S, Ser; T, Thr; V, Val; W, Trp; and Y, Tyr.

provided that the peptide was long enough to directly interact with SdrG's locking strand, forces were still in the nN regime (Fig. 3A). Removing all residues contacting the locking strand up to Fgβ's A13 eliminated clear complex rupture forces in the nN regime. Consequently, the minimal six-residue peptide sequence in closest contact with the locking strand (FFSARG) was sufficient to both bind SdrG and withstand forces indistinguishable from WT Fgβ in vitro (Fig. 3B and fig. S5C).

Provided a mutant could still bind SdrG, modifying the Fgβ peptide had only minor effects on mechanostability. Thus, we investigated the mechanical properties of SdrG. Previously, the presence and flexibility of the locking strand was shown to be crucial for the DLL mechanism and thus SdrG:Fgβ affinity (*25*). Locking strand deletion inhibits binding of Fgβ (*4*). In accordance with these results, a mutant SdrG(274-580) devoid of the locking strand failed to bind Fgβ in vitro. Still, the contribution of the locking strand to the mechanics was unclear. If the interaction between the N2 domain and the locking strand propagated force away from the complex, its truncation should significantly weaken rupture forces. A truncated SdrG(274-590)—which removed the locking strand's C-terminal half of the "latch" region (fig. S6)—still bound SdrG, yet its mechanostability was indistinguishable from the WT. Possible covalent isopeptide bonds (*27*, *28*) between the locking strand and the N2 domain had been suggested to contribute to its stability. We could exclude this hypothesis as cause of the unusually high mechanostability because the SdrG truncation mutant removed D593, a key amino acid required for a potential isopeptide bond (*29*).

As simulations and experiments strongly agreed, we were confident to explore mutants and setups created in silico that could not be realized in vitro. SMD became a gedankenexperiment to deconstruct the mechanism. It is important to emphasize that the strong agreement was provided in part by our enhanced sampling strategy (*30*). Performing many (at least 50 per system, more than 2400 total; see overview in table S1) simulation replicas allowed the comparison of simulation and experiment within the same theoretical framework of the Bell-Evans (BE) and Dudko-Hummer-Szabo (DHS) models (*24*, *31*, *32*).

Simulations revealed the presence of strikingly frequent and persistent hydrogen bonds (H bonds) between the Fgβ peptide backbone and SdrG (Fig. 3, D and F, and figs. S7 and S8). We investigated the contribution of the backbone H bonds in SMD simulations by replacing Fgβ with a polyglycine peptide, which has no side chains. In silico, the rupture forces were merely 27% weaker than the WT, comparable to the FgβF0 mutant (Fig. 3E). Thus, we updated our initial hypothesis: Reaching the regime of 2 nN was largely independent of Fgβ's side chains and mainly caused by SdrG interacting with the Fgβ peptide backbone (figs. S9 and S10). Breaking the SdrG:Fgβ complex in the native configuration requires all H bonds to be broken in parallel: a cooperative shear geometry (see movie S1).

Similar shear geometries appear in folds such as the muscle protein titin-Ig. However, this protein unfolds at lower forces around 200 pN (*33*), in stark contrast to SdrG's over 2000 pN. The shear geometry in titin breaks because its backbone H bonds have the freedom to move orthogonally to the force load, ultimately circumventing the shear geometry (*34*). In the SdrG:Fgβ complex, the peptide is snugly confined in the interface between N2 and N3 domain by the locking strand (figs. S10 and S11). The rigid and coiled (Fig. 3C and fig. S12) alignment of the two interacting backbones neither bends nor buckles. Peptide movement orthogonal to the pulling force vector is not possible, so all H bonds must be broken at once. The importance of this packed confinement was also demonstrated by analyzing the correlation-based dynamical network (*35*), which shows how force propagates through the system (fig. S13) and how atom motion is clustered in communities (fig. S14). These analyses revealed that force is propagated not directly by the latch strand, as demonstrated experimentally, but by neighboring strands, reducing the load over the H bonds. Notably, the movement of the Fgβ peptide and both the N2 and N3 domain were highly correlated. To demonstrate the importance of the correct H-bond alignment, Fgβ was tethered non-natively from its N terminus, effectively pulling orthogonally to the native force propagation. The non-native pulling of Fgβ peaked at forces around 60 pN (Fig. 4A), smaller than the native configuration by a factor of more than 40 (fig. S15). Simulations showed that this geometry is weaker, because the interactions between N2 and N3 are broken, resulting in a loss of peptide confinement (see figs. S16 and S17, and movie S2).

In a simplified model, the DLL mechanism creates a deep and rigid binding pocket for the peptide, which is confined in a coiled geometry similar to a corkscrew in a cork (figs. S12 and S18). If pulled upon, the load is dissipated cooperatively over all H bonds that are radially pointed outward of Fgβ (Fig. 3G), causing the high mechanostability.

The importance of these H bonds was confirmed in an exploratory SMD through removing coulomb interactions from parts of the peptide required for hydrogen bonding. Eliminating backbone H bonds resulted in a significant reduction in rupture force in silico (Fig. 3E). Additionally, eliminating hydrogen bonds formed by the side chains of Fgβ further reduced the forces, but only marginally, in agreement with the mechanism proposed (Fig. 3E). Still, the forces observed were only about 40% smaller than the WT. Furthermore, we tested turning off H bonds of the all-glycine peptide, which finally led to

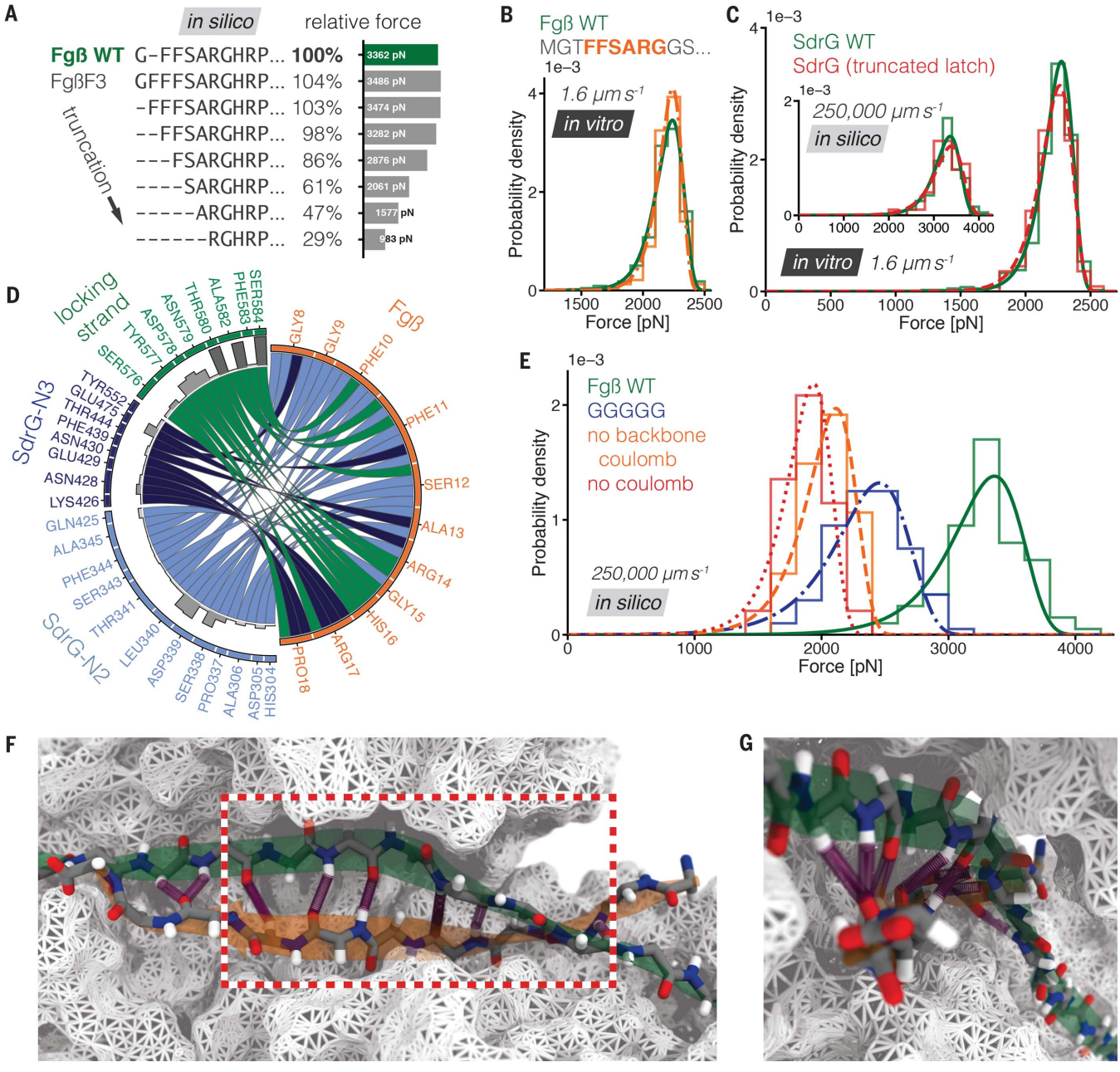

Fig. 3. Backbone H bonds are deciding factors in the high mechanostability of SdrG:Fgβ and a minimized peptide. (**A**) Fgβ peptide truncations from the N terminus in silico. Removing amino acids causes the forces to drop (relative to the WT), with the most significant drop when removing the sequence FSAR, leading to FFSARG as the minimum peptide. (**B**) Rupture forces for SdrG binding to WT Fgβ (green, continuous line, N = 437), and the six-residue minimized peptide FFSARG (orange, dash-dotted line, here shown with surrounding amino acids in gray, N = 471). Strikingly, there is hardly any difference between WT Fgβ and the minimized peptide. (**C**) Rupture-force histograms comparing the WT Fgβ:SdrG interaction (green, continuous line, N = 463) and the SdrG mutant with the truncated latch region (red, dashed line, N = 131). WT and mutant are virtually indistinguishable (no significant difference in Kolmogorov-Smirnov test, in vitro P = 0.29, in silico P = 0.88). Corresponding SMD results (WT N = 100, mutant N = 50) are shown as inset. (**D**) Relative prevalence (bar graphs; precise values in fig. S7) of H bonds between SdrG domains, the locking strand, and the WT Fgβ peptide (also available for F3, F1, F0, and all-glycine mutants in fig. S8). The locking strand connects to nearly every Fgβ residue. (**E**) Rupture forces from exploratory simulations for SdrG and Fgβ WT (green, continuous line, N = 100), a replacement of each Fgβ residue with glycine (blue, dash-dotted line, N = 100), FgβF3 peptide without coulomb interactions, and subsequently H bonds, on its backbone (orange, dashed line, N = 47), FgβF3 devoid of all coulomb interactions (red, dotted line, N = 48). Backbone H bonds in the Fgβ confinement allow even a pure glycine sequence to withstand high force. (**F**) H-bond (purple) contacts respective to the backbone of Fgβ (orange) and locking strand (green) confined by SdrG (white surface) from simulations in a force-loaded state. The minimum peptide sequence is highlighted in the red box. (**G**) Radial distribution of backbone H bonds between locking strand (green) caused by the screwlike winding of the Fgβ sheet (orange). Peptide backbones are shown as sticks.

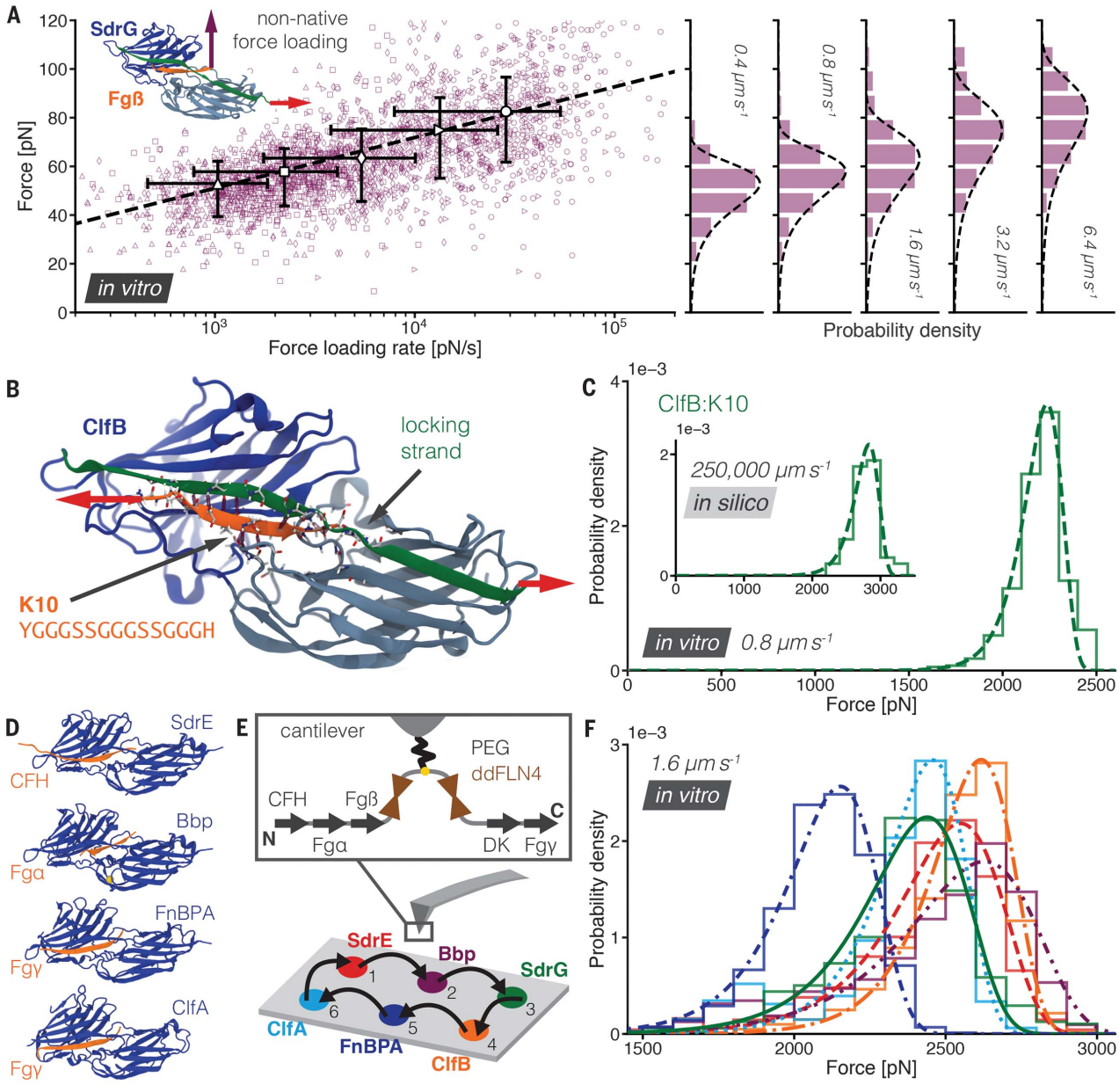

Fig. 4. A non-native SdrG:Fgβ force loading shows weak forces, a homologous domain ClfB reaches 2 nN stability binding a mainly glycine-serine peptide, and SdrG homologs consistently exceed 2 nN binding to their ligands. (**A**) Dynamic force spectrum of the SdrG:Fgβ non-native configuration (see inset with purple arrow), breaking around 60 pN as opposed to >2 nN for the native case (for SMD results, see figs. S15 to S17 and movie S2). Cantilever retraction velocities were varied: 0.4 µm s^{-1} (triangles, N = 511), 0.8 µm s^{-1} (squares, N = 564), 1.6 µm s^{-1} (diamonds, N = 487), 3.2 µm s^{-1} (forward triangles, N = 395), 6.4 µm s^{-1} (circles, N = 471), with corresponding complex rupture-force histograms projected on the right. A BE model fit (dashed line) through the most-probable rupture force and force loading rate of each velocity (large open markers) shows the expected force loading-rate dependency of the rupture force (Δx = 0.46 nm, k_{off}^0 = 0.39 s^{-1}). (**B**) ClfB (blues):K10 (orange) complex, including the locking strand (green) and H-bonding (purple) amino acids, shown as sticks. Notably, the latch region was not crystallized and needed to be modeled from a homolog. The native pulling configuration is indicated with an arrow; compared with Fgβ, the peptide is oriented inversely in the binding pocket. (**C**) Rupture-force histogram and fit for ClfB:K10 at a velocity of 0.8 µm s^{-1} (green, dashed line, N = 1035), peaking around 2.3 nN. Simulation data (N = 50) confirming the force regime are shown as inset. (**D**) Homologous systems employing the DLL mechanism, all from *S. aureus* (N2 and N3 domains in blue, target peptides in orange) SdrE, Bbp, FnBPA, and ClfA. (**E**) Comparison of absolute mechanostability of all homologous systems, as well as SdrG and ClfB, with a single force probe. The cantilever is modified with five different peptides tethered in their native force loading geometry, respectively: from the C terminus of complement factor H (CFH), Fgα chain (Fgα), and Fgβ, tethered from the N terminus are sequences from dermokine (DK) and Fgγ chain (Fgγ). This selection is presented to all adhesins, which are known to bind at least one of them, spatially separated on a surface. One cannot exclude that one adhesin may bind more than one peptide target. (**F**) Resulting relative stabilities of the complexes for SdrE (red, dashed line, N = 680), ClfB (orange, dash-dotted line, N = 605), ClfA (cyan, dashed line, N = 2292), Bbp (purple, dot-dot-dashed line, N = 319), SdrG (green, continuous line, N = 478), FnBPA (blue, dash-dash-dotted line, N = 2483). SdrG is not the strongest system at a retraction velocity of 1.6 µm s^{-1}. In accordance with the largely side-chain independent mechanics proposed for SdrG and ClfB, every DLL adhesin withstands forces exceeding 2 nN.

no detectable peak in the force profile. H bonds with the peptide backbone were key to the mechanostability.

A pure glycine sequence—i.e., no side chains—showed high forces when bound to SdrG in silico. An analogous experiment was not possible, because such a sequence did not bind SdrG. The side chains, such as the hydrophobic phenylalanine residues, were not essential for mechanostability but were crucial for affinity. A homologous DLL motif adhesin, clumping factor B (ClfB) from *S. aureus,* had been found to promiscuously bind short sequences of extracellular matrix proteins. Among its targets is a C-terminal cytoskeletal keratin peptide (K10, YGGGSSGGGSSGGGH) (*5*). This unusually unremarkable target is essentially a flexible linker terminating in a charged residue. K10 contains no bulky, charged, or hydrophobic side chains, except for the C-terminal histidine, secured by the locking strand in the complex structure. ClfB:K10 interactions also exceed the 2 nN mark, both in vitro and in silico (see Fig. 4, B and C). More prominently than in SdrG, ClfB's mechanostability must be based on H bonds to the K10 backbone, simply because it has no notable side chains. In last consequence, even a shortened K10 and pure GS sequence (GGGSSGGGSSGGG) binds ClfB and reaches more than 2nN in force (fig. S19). Moreover, the peptide β sheet is parallel to the locking strand, whereas the orientation is antiparallel in SdrG. Accordingly, it was natively tethered from its N terminus, showing that nN stability is also possible for an inversely oriented peptide configuration. Finally, to generalize the mechanics, we probed four additional homologs of SdrG and ClfB, all from *S. aureus*. SD repeat protein E (SdrE), clumping factor A (ClfA), bone sialoprotein binding protein (Bbp), and fibronectin binding protein A (FnBPA) had been crystallized with a known ligand bound (Fig. 4D) (*36*–*39*). Although most-probable rupture forces varied up to 20% depending on the adhesin, the overall forces were consistently in the 2 nN regime (Fig. 4, E and F).

Side-chain independent mechanics confer an invasive advantage to staphylococci. No matter which sequence is targeted by their adhesins, invading pathogens using the DLL mechanism can adhere to their hosts even under the most demanding mechanical stress. One could speculate that this mechanism provides a flat fitness landscape. Adaption to a target will automatically yield extremely resilient mechanics, even if the sequence is mainly glycines and serines. The moderate bulk affinity of SdrG:Fgβ allows for flexible unbinding and rebinding when no mechanical stress is applied. One could further speculate that a high-complex lifetime under force, which seems probable given the overall extreme mechanostability, is indicative of a very different unbinding pathway when compared with the moderate lifetimes of spontaneous unbinding in bulk experiments (*4*). Thus, these differing pathways would make a catch-bond behavior not surprising, considering that such bonds have been found in bacterial adhesins with similar functions, albeit much lower mechanical strength (*40*, *41*).

In conclusion, SdrG:Fgβ and its homologs are the mechanically strongest noncovalent protein-protein receptor-ligand interactions to date, rivaling a regime formerly exclusively associated with covalent bonds. The DLL mechanism creates a deep and rigid binding pocket confining the target in a stable geometry that mainly relies on backbone H bonds. Hence, the mechanostability of the complex only marginally depends on the target side chains and thus sequence, even if it is minimized to merely six amino acids. These adhesins are hyperstable protein handles suitable for mechanochemistry and able to unfold almost any protein. They may serve as templates to design even stronger ones—a noncovalent superglue (*42*, *43*). The mechanism proposed provides an atomistic understanding of why these adhesins can adhere to their hosts so resiliently, from which possible routes to inhibit it and impede staphylococcal adhesion may be derived.

REFERENCES AND NOTES

1. T. J. Foster, J. A. Geoghegan, V. K. Ganesh, M. Höök, *Nat. Rev. Microbiol.* **12**, 49–62 (2014).
2. M. Otto, *Nat. Rev. Microbiol.* **7**, 555–567 (2009).
3. C. C. S. Deivanayagam *et al.*, *EMBO J.* **21**, 6660–6672 (2002).
4. K. Ponnuraj *et al.*, *Cell* **115**, 217–228 (2003).
5. V. K. Ganesh *et al.*, *J. Biol. Chem.* **286**, 25963–25972 (2011).
6. J. A. Sharp *et al.*, *PLOS ONE* **7**, e38407 (2012).
7. T. J. Foster, M. Höök, *Trends Microbiol.* **6**, 484–488 (1998).
8. Y. Zong *et al.*, *EMBO J.* **24**, 4224–4236 (2005).
9. S. L. Davis, S. Gurusiddappa, K. W. McCrea, S. Perkins, M. Höök, *J. Biol. Chem.* **276**, 27799–27805 (2001).
10. H. Breithaupt, *Nat. Biotechnol.* **17**, 1165–1169 (1999).
11. J. A. Geoghegan, T. J. Foster, P. Speziale, Y. F. Dufrêne, *Trends Microbiol.* **25**, 512–514 (2017).
12. D. J. Müller, Y. F. Dufrêne, *Nat. Nanotechnol.* **3**, 261–269 (2008).
13. V. Vogel, M. Sheetz, *Nat. Rev. Mol. Cell Biol.* **7**, 265–275 (2006).
14. H. Yu, M. G. W. Siewny, D. T. Edwards, A. W. Sanders, T. T. Perkins, *Science* **355**, 945–950 (2017).
15. P. Herman *et al.*, *Mol. Microbiol.* **93**, 356–368 (2014).
16. T. Vanzieleghem, P. Herman-Bausier, Y. F. Dufrene, J. Mahillon, *Langmuir* **31**, 4713–4721 (2015).
17. P. Vitry *et al.*, *mBio* **8**, e01748–e17 (2017).
18. P. Herman-Bausier *et al.*, *mBio* **7**, e01529–e16 (2016).
19. C. Schoeler *et al.*, *Nat. Commun.* **5**, 5635 (2014).
20. R. Merkel, P. Nassoy, A. Leung, K. Ritchie, E. Evans, *Nature* **397**, 50–53 (1999).
21. M. Grandbois, M. Beyer, M. Rief, H. Clausen-Schaumann, H. E. Gaub, *Science* **283**, 1727–1730 (1999).
22. I. Schwaiger, A. Kardinal, M. Schleicher, A. A. Noegel, M. Rief, *Nat. Struct. Mol. Biol.* **11**, 81–85 (2004).
23. F. Rico, L. Gonzalez, I. Casuso, M. Puig-Vidal, S. Scheuring, *Science* **342**, 741–743 (2013).
24. O. K. Dudko, G. Hummer, A. Szabo, *Phys. Rev. Lett.* **96**, 108101 (2006).
25. M. G. Bowden *et al.*, *J. Biol. Chem.* **283**, 638–647 (2008).
26. J. V. Ribeiro *et al.*, *Sci. Rep.* **6**, 26536 (2016).
27. M. Walden *et al.*, *eLife* **4**, 1–24 (2015).
28. J. Alegre-Cebollada, C. L. Badilla, J. M. Fernández, *J. Biol. Chem.* **285**, 11235–11242 (2010).
29. U. Sridharan, K. Ponnuraj, *Biophys. Rev.* **8**, 75–83 (2016).
30. R. C. Bernardi, M. C. R. Melo, K. Schulten, *Biochim. Biophys. Acta* **1850**, 872–877 (2015).
31. E. Evans, K. Ritchie, *Biophys. J.* **72**, 1541–1555 (1997).
32. S. Izrailev, S. Stepaniants, M. Balsera, Y. Oono, K. Schulten, *Biophys. J.* **72**, 1568–1581 (1997).
33. M. Rief, M. Gautel, F. Oesterhelt, J. M. Fernandez, H. E. Gaub, *Science* **276**, 1109–1112 (1997).
34. H. Lu, K. Schulten, *Biophys. J.* **79**, 51–65 (2000).
35. C. Schoeler *et al.*, *Nano Lett.* **15**, 7370–7376 (2015).
36. X. Zhang *et al.*, *Protein Cell* **6**, 757–766 (2015).
37. Y. Zhang *et al.*, *Biochem. J.* **474**, 1619–1631 (2017).
38. V. Stemberk *et al.*, *J. Biol. Chem.* **289**, 12842–12851 (2014).
39. V. K. Ganesh *et al.*, *PLOS Pathog.* **4**, e1000226 (2008).
40. W. E. Thomas, V. Vogel, E. Sokurenko, *Annu. Rev. Biophys.* **37**, 399–416 (2008).
41. M. M. Sauer *et al.*, *Nat. Commun.* **7**, 10738 (2016).
42. G. Veggiani, B. Zakeri, M. Howarth, *Trends Biotechnol.* **32**, 506–512 (2014).
43. T. Verdorfer *et al.*, *J. Am. Chem. Soc.* **139**, 17841–17852 (2017).

ACKNOWLEDGMENTS

We thank T. Nicolaus and A. Kardinal for laboratory assistance; E. Durner, M. A. Jobst, W. Ott, and T. Verdorfer for work on instrumentation and surface chemistry; M. C. R. Melo for assistance with correlation-based network analysis; M. Scheurer for assistance with PyContact; and H. Clausen-Schaumann, Daniel Müller, and Z. Luthey-Schulten for helpful discussions. **Funding:** We gratefully acknowledge funding from an advanced grant of the European Research Council (ERC, Cellufuel Grant 294438) and from the Deutsche Forschungsgemeinschaft (DFG, Sonderforschungsbereich 1032). This work was supported by National Institutes of Health (NIH) grant P41-GM104601, "Center for Macromolecular Modeling and Bioinformatics." R.C.B. is partially supported by National Science Foundation (NSF) grant MCB-1616590, "Molecular Modeling of Bioenergetic Systems." Molecular dynamics simulations made use of GPU-accelerated nodes of Blue Waters supercomputer as part of the Petascale Computational Resource (PRAC) grant "The Computational Microscope," which is supported by the National Science Foundation (award numbers ACI-1440026 and ACI-1713784). Blue Waters sustained-petascale computing project is supported by the National Science Foundation (awards OCI-0725070 and ACI-1238993) and the state of Illinois. **Author contributions:** R.C.B., H.E.G., K.S., and L.F.M. conceived the research and interpreted the results; L.F.M. performed all experiments; R.C.B. performed all simulations; R.C.B., H.E.G., and L.F.M. wrote and revised the manuscript. **Competing interests:** The authors declare no competing interests. **Data and materials availability:** Key plasmids are available on Addgene; see the supplementary materials for identifiers.

SUPPLEMENTARY MATERIALS

www.sciencemag.org/content/359/6383/1527/suppl/DC1
Materials and Methods
Figs. S1 to S19
Table S1
Movies S1 and S2
References (*44*–*71*)

13 October 2017; accepted 1 March 2018
10.1126/science.aar2094

Science

Molecular mechanism of extreme mechanostability in a pathogen adhesin

Lukas F. Milles, Klaus Schulten, Hermann E. Gaub and Rafael C. Bernardi

Science **359** (6383), 1527-1533.
DOI: 10.1126/science.aar2094

How a pathogen holds on to its host

Staphylococcus epidermidis and *Staphylococcus aureus* are pathogens that can form biofilms on implants and medical devices. Central to biofilm formation is a very tight interaction between microbial surface proteins called adhesins and components of the extracellular matrix of the host. Milles *et al.* used atomic force microscopy-based single-molecule force spectroscopy combined with steered molecular dynamics to explore how the bond between staphylococcal adhesin SdrG and its target fibrinogen peptide can withstand forces greater than 2 nanonewtons (see the Perspective by Herman-Bausier and Dufrêne). The peptide is confined in a coiled geometry in a deep and rigid pocket through hydrogen bonds between SdrG and the peptide backbone. If pulled, the load is distributed over all hydrogen bonds so that all bonds must be broken at once to break the interaction.

Science, this issue p. 1527; see also p. 1464